Received December 5, 2017, accepted January 21, 2018, date of publication February 16, 2018, date of current version April 18, 2018.

Digital Object Identifier 10.1109/ACCESS.2018.2806885

The Development of Low-Current Surface Arcs Under Clean and Salt-Fog Conditions in Electricity Distribution Networks

XIN ZHANG[1,2], (Member, IEEE), JIEBEI ZHU[3], (Member, IEEE), SIQI BU[4], (Senior Member, IEEE), QI LI[1], (Member, IEEE), VLADIMIR J. TERZIJA[2], (Fellow, IEEE), AND SIMON M. ROWLAND[2], (Fellow, IEEE)

[1]Electricity National Control Centre, National Grid UK, Wokingham RG41 5BN, U.K.
[2]School of Electrical and Electronic Engineering, The University of Manchester, Manchester M13 9PL, U.K.
[3]School of Electrical and Information Engineering, Tianjin University, Tianjin 300072, China
[4]The Hong Kong Polytechnic University, Hong Kong

Corresponding author: Xin Zhang (xin.sam.zhang@gmail.com)

ABSTRACT Electricity distribution networks are built to deliver increasing amount of electricity from distributed energy resources (DERs) such as offshore and onshore wind and solar farms. Aging of network assets through low-current surface discharges is becoming a great concern for the security and reliability of the distributed energy supply. In particular coastal conditions can present a challenge for overhead line insulators through the environment of salt fog. Also, onshore areas may expose power lines to clean fog and agricultural or industrial pollution. In this paper, experimental studies are conducted to investigate electrical arc formation and growth on insulators, following the testing standards in accordance with IEC 61109. Dry-band arcs in both clean-fog and salt-fog environments are compared. It is identified that arcs are much faster to develop and have greater energy in salt-fog environments, due to the lower surface resistance and resulting higher leakage current. The time from a first arc to strike, to the situation where the arc is stable on the insulator surface is identified as a potentially critical parameter in controlling aging of an insulation surface. The time from initial appearance of an arc to full stability is eight times shorter in a salt fog of 16,000 μS/cm compared to a clean fog of 600 μS/cm. This means the very existence of a stable low-current arc is much more likely in polluted conditions. Accumulated arc energy and heat dissipation have been calculated for both fog conditions. It is concluded that aging by low-current electrical arcs tends to be more severe in salt-fog environments, so that great care needs to be taken when designing overhead lines and insulators in such areas.

INDEX TERMS Arc discharges, insulators, accelerated aging, power dissipation, salt fog, clean fog, dry-band arc, leakage current, distribution network, non-ceramic insulator, composite insulator.

I. INTRODUCTION

Aging of outdoor insulation under low amplitude leakage currents is a concern for the long-term reliability of electricity distribution networks. Overhead line elements such as insulators and ADSS (All Dielectric, Self-Supporting) cables are subject to electric fields, leakage currents, and resulting surface discharges such as dry-band arcs [1]–[3]. Electrical arcs lead to erosion and chemical damage thereby reducing the reliability of polymeric insulation materials [4], [5]. This may eventually lead to the mechanical failure of composite insulators, contributing to transmission line faults [6], [7].

Moisture in an outdoor environment contributes to the electrical discharge process by reducing surface resistance and distorting local electric fields [8]. It can also lower the threshold voltage for flashover [9], [10]. Fog is a major source for moisture deposition on transmission line assets. In particular, research on arc formation and polymer aging has been reported in both clean fog [11]–[13] and salt fog [14]–[16], but with limited comparison between the two [17]. Furthermore, special care needs to be taken when designing or selecting insulators for offshore or contaminated areas where salt fog is prevalent. This should be considered as a different aging environment from clean-fog areas, especially for the growth of electrical discharges. For this reason, understanding the development of electrical arcs in different fog environments becomes necessary.

In this paper, insulation samples are tested in both clean-fog and salt-fog environments. Studies focus on the development of low-current arcs, and the features of arc voltage, current and energy of both tests are compared. Accumulated heating effects from the arc on the insulation surface are also compared. More severe aging has been observed from electrical arcs in the salt-fog environment.

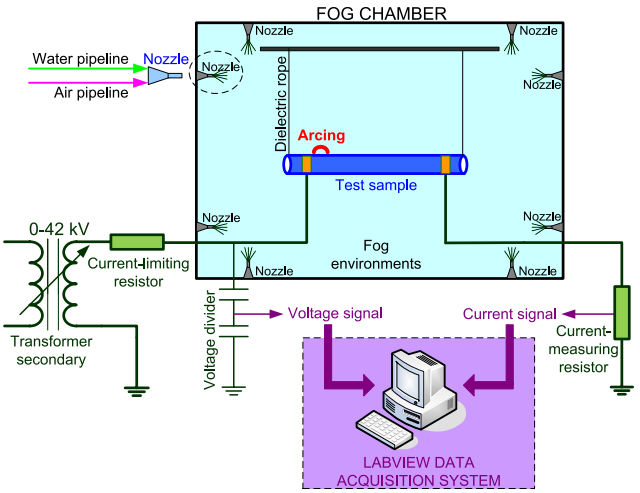

FIGURE 1. Test arrangement to enable voltage and current measurements of low-current arcs in fog environments.

II. EXPERIMENTAL SET-UP AND TEST PROCEDURE

A. TEST ARRANGEMENT

Figure 1 illustrates the arrangement for testing in a fog environment. The transformer provided single-phase AC voltage up to 42 kV at its secondary side. A current-limiting resistor (representing the passive surface resistance of an insulator surface) was used to limit the leakage current to less than 10 mA. A 60 cm long, commercially manufactured fibre-glass reinforced rod sheathed in silicone rubber was used as the test sample. This structure, which represents a typical composite insulator core without sheds, was used to simplify the test. The sample was suspended horizontally in the fog chamber, with the high voltage end connected to the transformer secondary via the current-limiting resistor, and the low voltage end attached to the earthed frame via a 1 kΩ current-measuring resistor. The horizontal sample layout allowed uniform and stationary moisture deposition. The profound impact of inclining the insulator to the horizontal, and enabling moisture movement on the surface, is reported elsewhere [18], [19]. The connections between the test circuit and sample were formed by wrapping copper strip tightly around the rod, with a separation of 50 cm.

The fog was generated in a sealed and waterproof chamber of dimensions 2.57 m × 2.57 m × 2.54 m (L × W × H), and a total volume of 16.8 m^3. A 1.25 m × 0.9 m glass window allowed visual observation of the experiment by the chamber operator, although a full fog can obscure the experiment. Six nozzles were placed around the internal wall of the chamber, fed from a compressed-air pipeline and a water pipeline. Air was supplied from a compressor with a maximum output of 100 psi. Water was pumped from a 220 litre tank filled with a solution to produce either clean water or salt water determined by the test specification. The salt-fog tests were in accordance with IEC 61109.

Control of the fog environment included fog precipitation rate and applied voltage. The air pressure regulator and pump valve controlled the fog injection. The precipitation rate was 6.7 ± 1.7 l/hr, with the air pressure set to 1 bar. Prior to running a test, the chamber precipitation rate was verified by accumulating deposits in an open-top vessel on the chamber floor. Voltage control was by a National Instrument Labview system controlling a motor to step up or down the rheostat feeding the transformer. A series of interlocks and over-current trip switches ensured safety and security.

The data measurement and acquisition system included a 10,000:1 voltage divider to measure the voltage across the sample. A 1 kΩ current measurement resistor was used to determine the leakage current flowing on the sample surface. Both voltage and current signals were recorded by Labview. A high speed video camera was used to capture the electrical discharge images.

B. TESTS IN CLEAN-FOG CONDITIONS

Clean fog was produced using Manchester tap water with conductivity of 600 μS/cm. The AC voltage was varied from 20 kV to 42 kV for each individual test. The current-limiting resistor was 2 MΩ. The sample surface was uniformly roughened with abrasive paper to reduce its surface hydrophobicity to encourage fog adhesion on the sample in a short time. The effects of continuous fog deposition and the high voltage gradient across the sample enabled a dry-band arc to form. The process typically took approximately three hours. The traces of arc voltage and current were measured and synchronized with arcing images.

C. TESTS IN SALT-FOG CONDITIONS

Salt fog was prepared from salt (NaCl) mixed with water to achieve a conductivity of 16,000 μS/cm. Otherwise the test conditions were replicated from the clean-fog case. Due to the high conductivity of the salt water deposited on the insulator, arcs tended to strike very quickly and were sustained for more than three hours with relatively stable arc lengths.

III. TEST RESULTS

A. ARC DEVELOPMENT IN CLEAN-FOG CONDITIONS

Figure 2 shows the measured voltage and current curves from the test inception to the condition of a stable arc being developed. Owing to the distorted shape of measured current profiles, and because it is the point-on-wave voltage that controls discharge properties [18], the leakage current or arc current is described by using peak values rather than RMS values. The following development stages have been identified:

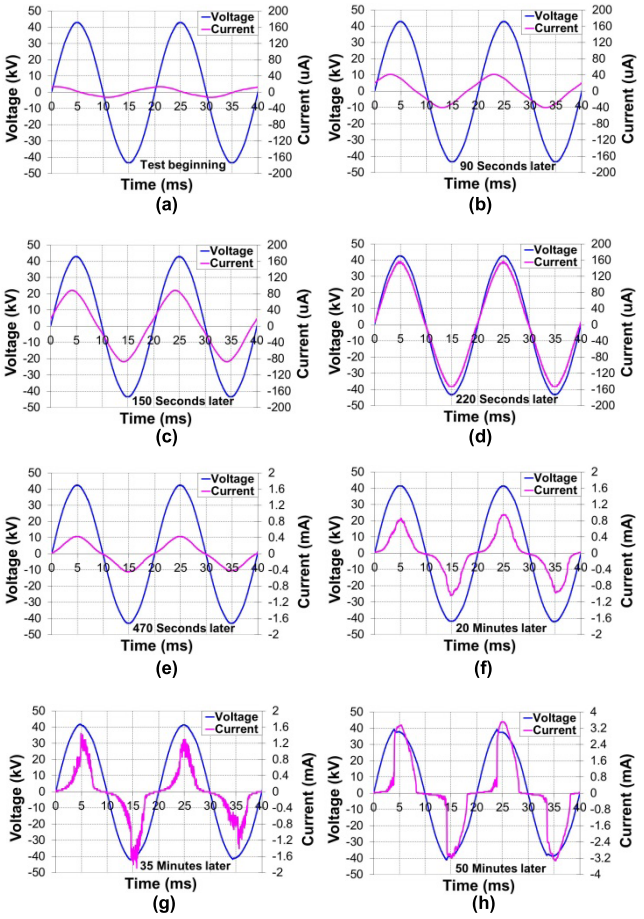

FIGURE 2. The voltage and current waveforms as a dry-band arc develops in a clean-fog test.

1. In the early stages, when the sample surface is still dry, the leakage current presents a peak value of 14 μA, which is low due to the excellent dielectric properties of silicone rubber. Also, the current leads the voltage by 90°, showing a capacitive characteristic as shown in Figure 2 (a).

2. After the sample surface has become wet due to fog deposition, the surface impedance reduces and the leakage current begins to grow. In the meantime, the leakage current gradually becomes in-phase with the voltage, shifting from capacitive (for the dry silicone rubber) to resistive (for the wetted surface) as seen in Figure 2 (b) and (c). The current and voltage traces are ultimately in phase with each other after 220 seconds, and the magnitude of leakage current significantly increases to 156 μA as shown in Figure 2 (d).

4. As the sample surface continues to become wetter forming a thicker layer of clean-fog deposit, the leakage current begins to distort after 470 seconds as shown in Figure 2 (e). Low-current discharges are present along with the current distortion, increasing the leakage current from 0.4 mA to 1.2 mA as shown in Figure 2 (e)-(g).

5. As the leakage current increases above 0.8 mA, dry-band arcs occur as shown in Figure 2 (f). Initially there are several unstable arcs striking on the sample surface, but finally one single arc dominates as shown in Figure 3. After approximately 50 minutes of the test running, the dry-band arc becomes stable with relatively constant length and repeatable voltage and current profiles for every power cycle as shown in Figure 2 (h).

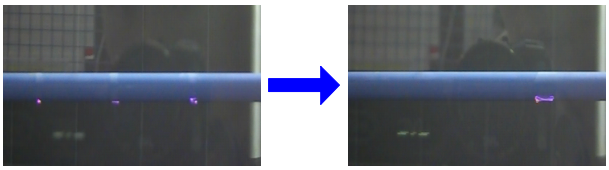

FIGURE 3. The transformation from several arcs to one single arc on the insulator surface in a clean fog. Images were taken at 20 mins and 50 mins into the test, associated with traces in Figure 2 (f) and (h).

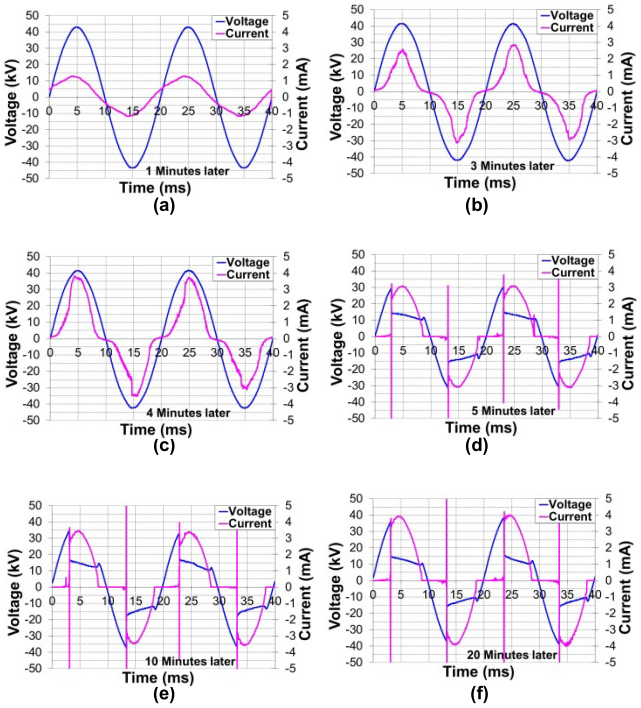

FIGURE 4. Arc development in a salt-fog test with arc (leakage) current rising from 1.5 mA to 4.0 mA.

B. ARC DEVELOPMENT IN SALT-FOG CONDITIONS

In the salt-fog tests, shifting of the relative phases between the voltage and current occurs in a similar way as in the clean-fog test. However, dry-band arcs tend to develop much quicker than in the clean fog, with an arc striking within 5 minutes of initial fog injection. Figure 4 records the current and voltage profiles for different stages of arc development:

1. The wetting process in the salt fog is similar to the clean-fog case, driven by the same fog precipitation rate. After approximately 1-2 minutes of water deposition, initial current distortion appears at a level of 1.5 mA in Figure 4 (a).

2. In the next few minutes, the peak leakage current rises to 3 mA as salt-water deposition increases on the insulation surface as shown in Figure 4 (b) and (c).

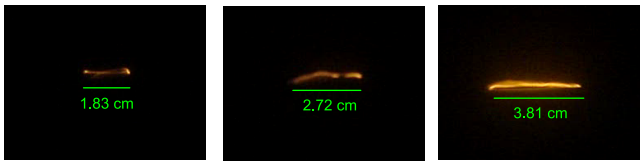

FIGURE 5. Arc growth from initial length of 18.3 mm to 38.1 mm in salt-fog test. Images were taken at 5 mins, 10 mins and 20 mins into the test, associated with traces in Figure 4 (d), (e) and (f).

3. Within 5 minutes after the start of the test, an initial arc strikes with a peak current of ∼3 mA, and the formation of a dry-band area begins as illustrated in Figure 4 (d). The arc current keeps growing to 3.5 mA as shown in Figure 4 (e).

4. After approximately 20 minutes, the arc current grows to a peak of 4 mA, and becomes stable (with a constant physical arc length) following the establishment of equilibrium as shown in Figure 4 (f). Images to record arc length from initial strike to full length are shown in Figure 5.

IV. ANALYSIS

A. CHANGE OF SURFACE PROPERTIES

In the first 220 seconds of the clean-fog test, the voltage and current traces were initially 90 degrees out of phase, and gradually became in phase, as shown in Figure 6.

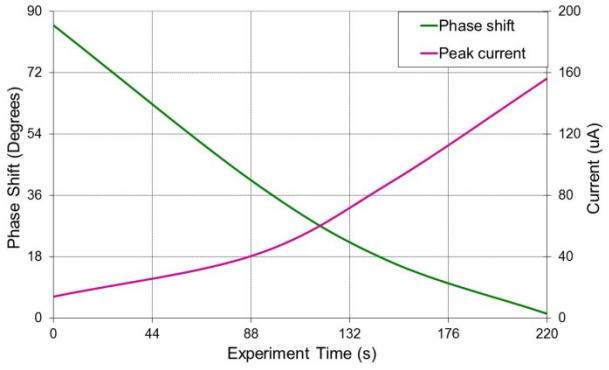

FIGURE 6. Summary of phase shift and current increase within 220 seconds in the clean-fog environment.

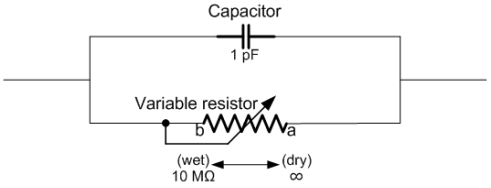

FIGURE 7. Electrical model of silicone rubber sample surface in dry and wet conditions.

In Figure 7, a simple electrical model is proposed to simulate the change of surface properties. The sample surface is represented by a capacitor parallel with a variable resistor. When the sample surface is still dry, the variable resistor taps at point 'a' with an extremely high value. The majority of leakage current is flowing through the capacitor, giving an initial dry current of 14 μA corresponding to a capacitance of ∼1 pF. The current leads the voltage at this stage. When the sample becomes wet due to fog deposition, the resistance drops dramatically, reaching its lowest value when the surface is fully wetted (around 6 MΩ for the clean-fog case). When a dry-band arc is present, the leakage current is limited by the series combination of the wet surface resistance (6 MΩ) and the arc resistance (4 MΩ).

Observations in the change of surface properties during the salt-fog test are similar. In this case, the wet surface resistance (0.85 kΩ) is relatively low due to the high conductivity of the salt solution.

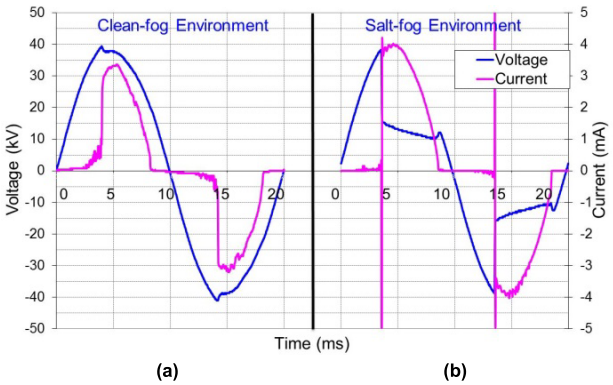

FIGURE 8. Voltage and current behavior of stable low-current dry-band arcs in: (a) clean fog, (b) salt fog.

B. ARC VOLTAGE AND CURRENT

Figure 8 shows the voltage and current traces of dry-band arcs in both clean-fog and salt-fog environments. For the salt-fog environment, the measured voltage during the arcing period drops significantly from 38 kV to 15 kV, but for the clean-fog environment, the measured arcing voltage does not fall dramatically when the arc is burning. The reason for the difference is that the voltage signal measured between the two ends of the sample includes the voltage across both the arc and wet surface. The salt-water surface yields a resistance as low as 0.85 kΩ. Because of the relatively high arc resistance of 4 MΩ, the salt-water surface only sees 0.02% of the measured voltage. In contrast, the resistance of the clean-water layer has a value of 6 MΩ, which takes up to 60% of the measured voltage. Therefore, the measured voltage in the clean fog is largely across the clean-water surface. As a result, the energy dissipated in the clean-water surface needs to be deducted when calculating arcing energy in the next section.

The arcing current is higher in the salt-fog environment compared to the clean fog as shown in Figure 8. This is due to the conductivity of the salt water on the surface which allows higher leakage current to flow. Therefore, the salt fog is a more severe aging environment for test samples.

The non-linear voltage-current (V-I) characteristics for dry-band arc development from 1.5mA to 4.0mA are shown in Figure 9. For each current level, V-I curves have symmetry across the positive and negative domains. In each half cycle

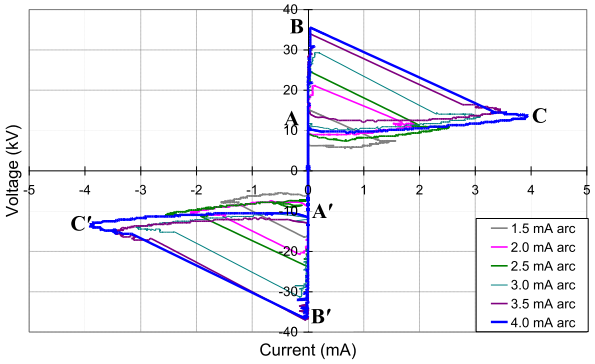

FIGURE 9. Voltage - current (V-I) characteristics of dry-band arcs for current levels from 1.5 mA to 4.0 mA in salt-fog tests.

the geometry of the V-I curves yield a triangular shape with: point B (B′ in the negative half cycle) identifying arc ignition, point C (or C′) the peak in current during the arc development, and point A (or A′) the point of arc extinction.

TABLE 1. Summary of arc formation time and time to arc stability.

Fog Type	Source Voltage	Arc Formation Time	Time to Arc Stability
Clean fog	42 kV	20 minutes	50 minutes
Salt fog	42 kV	5 minutes	20 minutes
Clean fog	32 kV	40 minutes	No stable arc after 2 hours
Salt fog	32 kV	5 minutes	20 minutes
Clean fog	20 kV	~ 1 hour	No stable arc after 3 hours
Salt fog	20 kV	5 minutes	30 minutes

Arc Formation Time: the time for an arc to form.
Time to Arc Stability: the time from its initiation for an arc to become stable.

C. ARC DEVELOPMENT TIME

Two defining time periods can be identified in the arc development: the time for the arc to form, and the time by which it becomes stable. The 'arc formation time' represents the period from applying the source voltage to striking the first arc. The 'time to arc stability' describes the period from the initial arc striking to creating a stable arc in terms of repeatable voltage and current profiles, and fixed physical length. A range of tests has been conducted in both clean-fog and salt-fog conditions under three different voltage levels. Results are summarized in Table 1. For each voltage level, salt fog encourages faster arc formation and stabilization than clean fog. This is due to the higher leakage current present along the conductive salt-water surface, leading to more rapid heating and formation of a dry-band area through Joule heating, and its stabilization by a higher current arc.

D. ARC POWER AND ENERGY

Instantaneous arc power is calculated in (1), based on the acquired voltage and current traces [18]. Figure 10 shows an

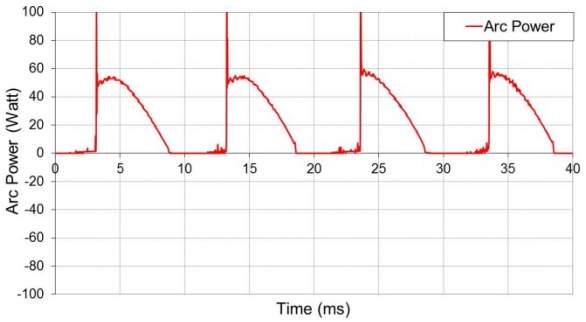

FIGURE 10. Instantaneous arc power for dry-band arc with 4 mA peak current in a salt fog.

example of calculated arc power for a 4.0 mA dry-band arc in the salt-fog test. The instantaneous arc power has non-linear characteristics given by:

$$p_a(t) = u_a(t) \times i_a(t) \tag{1}$$

where $p_a(t)$ is the instantaneous power of the arc, $u_a(t)$ is the measured arc voltage, and $i_a(t)$ is the measured arc current.

Arc energy per cycle is calculated based on the instantaneous arc power as shown in (2). The data acquisition system makes 800 discrete measurements per cycle length of 20 ms. The cycle contains two peaks of arc power [19]. E_{cycle} , the arc energy per cycle, is given by:

$$E_{cycle} = \sum_{n=1}^{800} (p_a(t_n) + p_a(t_{n+1})) \times t_n \tag{2}$$

where $p_a(t_n)$ is the instantaneous arc power at the n^{th} sample point, and t_n is the interval sampling period of 0.025 ms.

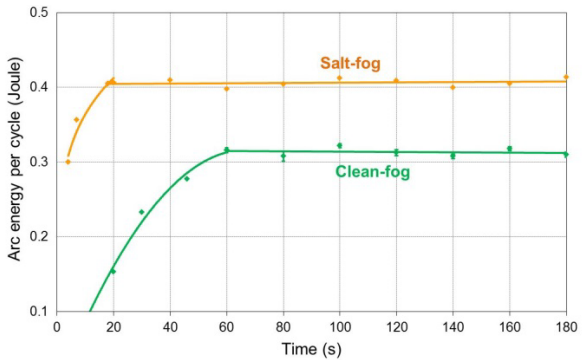

FIGURE 11. The development of arc energy per cycle in clean-fog and salt-fog environments; Source voltage is 42kV.

Figure 11 shows the development of arc energy (per cycle) as time elapses in both clean-fog and salt-fog environments. The actual voltage across the arc in the clean-fog case was calculated from the measured voltage, compensating for the wet surface resistance as discussed previously. Under the same source voltage, arcs in salt fog produce higher energy than in clean fog. This is due to the salt water allowing higher arc current. When the arc first appears in the salt fog, it has already developed 60% of its maximum energy per cycle, and reaches its maximum value in less than 20 minutes. This

may be due to the large leakage current and high voltage gradient across the dry-band area, which accelerates the arc development process. In contrast, arc energy in the clean fog tends to develop gradually. From the initial strike to full energy takes over 50 minutes. This is caused by lower conductivity in clean water, limiting the leakage current and voltage gradient across the dry band.

Eventually, arc energy tends to reach equilibrium in both clean-fog and salt-fog tests, which represents a stable equilibrium between arc heating evaporating water and water deposition from the fog.

V. DISCUSSION

A. ACCUMULATED ARC ENERGY IN DIFFERENT FOG ENVIRONMENTS

Experimental observation indicates that a dry-band arc can be sustained for a fairly long period (minutes or even hours) if equilibrium is achieved on the insulator surface between the arc and fog environment. Also the test surface is robust against the aging processes for many hours. It is considered that accumulated arc energy is a major aging parameter for the material surface, due to the amount of heat and UV radiation being generated at the fixed location. Equation (3) calculates the total accumulated energy as time elapses:

$$E_{accum}(t) = \int_0^T E_{cycle}(t)\,dt \tag{3}$$

where $E_{accum}(t)$ is the total accumulated energy of a dry-band arc at time t over a period T, and E_{cycle} is the arc energy per cycle.

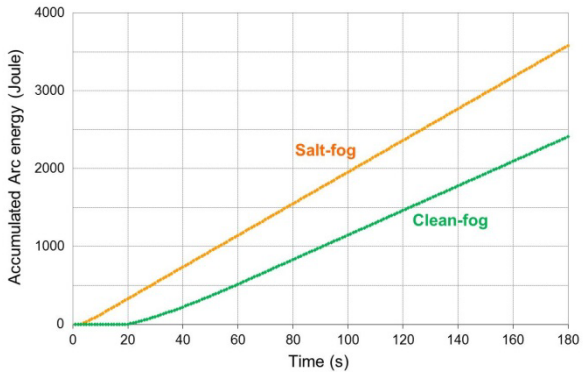

FIGURE 12. Accumulated arc energy in clean-fog and salt-fog conditions.

Figure 12 shows the accumulated arc energy calculation for both clean fog and salt fog. The calculation is based on the discrete sampling points of $E_{cycle}(t)$ every 20 seconds. Results clearly indicate that an arc in a salt-fog environment tends to convert more energy than in a clean fog. Therefore as time elapses, arcs in salt fog may be expected to produce more damage on an insulator's surface due to the higher energy accumulation.

A second point to note is that energy is generated rapidly in arcs in the salt-fog case, suggesting that even short adventitious periods will lead to a contribution to damage in polluted conditions. On the other hand, some time is required to generate the conditions for stable arcs in a clean fog, and this decreases the likelihood of damage occurring even if arcs are initiated. This highlights the importance of 'the time to arc stability'.

B. ARC ENERGY DISSIPATION

To further investigate the power flow inside the dry-band arc and from the arc to its surroundings, the physical geometry of an arc is modeled as a cylinder as shown in Figure 13. This approach was developed for the investigation of high current (~500 A), low voltage (~20 V), and short (< 6 mm) arcs between metal contacts in switchgear [20]. In this paper, such a model is applied for the first time to dry-band arcs with low current (1-5 mA), high voltage (10-25 kV) and between water electrodes. A concentrated heat source of arc power $P_a(t)$, previously defined in (1), is located in the geometrical center of the cylinder, and dissipates heat energy to both the cylinder's curved surfaces and planar faces.

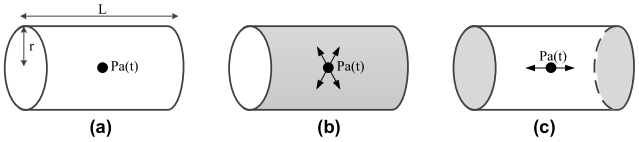

FIGURE 13. Power flow calculation in a cylinder model of a dry-band arc.(a) Cylindrical surface with a concentrated power source at its centre, $P_a(t)$. (b) Power flowing through the cylinder's curved surface. (c) Power flowing through the cylinder's planar faces.

As illustrated in Figure 13 (b), the instantaneous power flowing through the cylinder's curved surface, as previously described in [20], is given by:

$$P_{surface}(t) = P_a(t)\frac{L/2}{\sqrt{r^2 + \left(L/2\right)^2}} \tag{4}$$

where $P_a(t)$ is the instantaneous arc power defined in (1), r is the cylinder radius, and L is the cylinder length (equivalent to arc length). As illustrated in Figure 13 (c), the power flowing through the cylinder planar faces, $P_{face}(t)$, also described in [20], is:

$$P_{face}(t) = P_a(t)\left(1 - \frac{L/2}{\sqrt{r^2 + \left(L/2\right)^2}}\right) \tag{5}$$

The cylinder radius r(t) of a dry-band arc is considered as a dynamic parameter varying with time t. The following is used to calculate r(t):

$$r(t) = K_L i_a(t) \tag{6}$$

where $i_a(t)$ is the instantaneous arc current, and K_L is a constant. A linear relationship is assumed so that a higher current corresponds to a thicker arcing zone. K_L can be determined from the maximum value of $r(t)_{max}$ and the measured peak arc current of $i_a(t)_{peak}$.

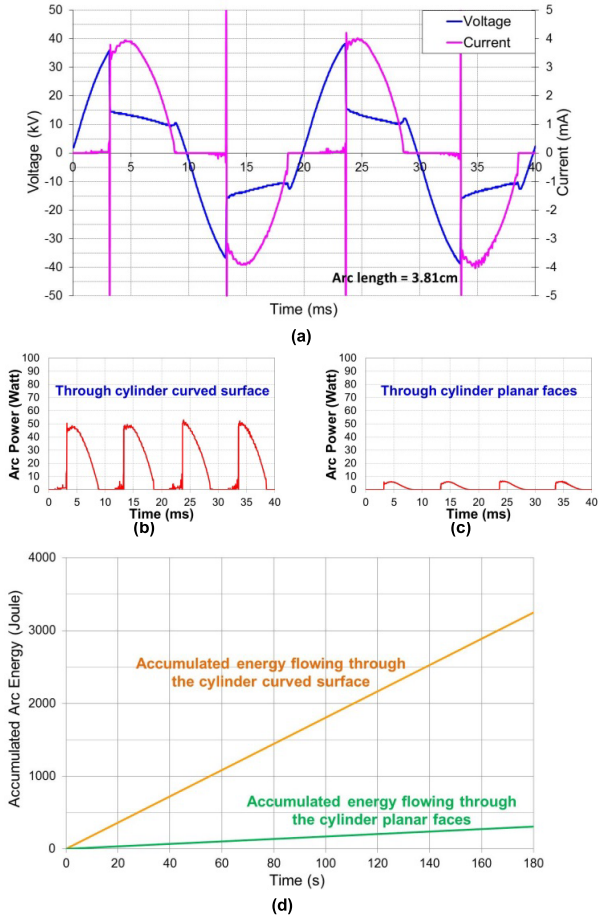

FIGURE 14. An example of arc power and energy dissipation through surfaces of the model of Figure 13: (a) Measured voltage and current traces from a dry-band arc. (b) Calculated arc power flowing through the arc cylinder curved surface. (c) Calculated arc power flowing through the arc cylinder planar faces. (d) Accumulated arc energy through the arc cylinder curved surface and planar faces.

An example is taken from the arc characteristics shown in Figure 14 (a). The ac source voltage with a peak value of 42 kV yielded a maximum arc current $i_a(t)_{max}$ of 4 mA. The thickness of the water layer was measured as 1 mm. $r(t)_{max}$ is taken as 1 mm from basic observations. However, the authors note the need for further study to develop this part of the model. Therefore the constant in (6), $K_L = \frac{r(t)_{max}}{i_a(t)_{peak}} = \frac{1\ mm}{4\ mA} = 0.25\ mm/mA$.

The arc power dissipation through the cylinder curved surface is calculated in (7), and the result is displayed in Figure 14 (b).

$$\begin{aligned} P_{surface}(t) &= P_a(t)\frac{L/2}{\sqrt{r(t)^2+\left(L/2\right)^2}} \\ &= u_a(t)\times i_a(t)\times\frac{38.1/2}{\sqrt{(0.25i_a(t))^2+\left(3.81/2\right)^2}} \end{aligned} \quad (7)$$

The arc power dissipation through two cylinder's planar faces is calculated in (8), and the result is displayed in Figure 14 (c).

$$\begin{aligned} P_{face}(t) &= P_a(t)\left(1-\frac{L/2}{\sqrt{r^2+\left(L/2\right)^2}}\right) \\ &= u_a(t)\times i_a(t) \\ &\quad\times\left(1-\frac{38.1/2}{\sqrt{(0.25i_a(t))^2+\left(3.81/2\right)^2}}\right) \end{aligned} \quad (8)$$

Finally, the arc energy per cycle $E_{surface}$ and E_{face} can be calculated based on $P_{surface}(t)$ and $P_{face}(t)$ using (2), yielding the results shown in Figure 14 (d).

Directional analysis in arc energy dissipation shows that the arc cylinder's curved surface transmits more than 90% of the total arc energy, whilst the cylinder's planar faces account for less than 10% of arc energy flow. This energy analysis shows that arc energy through the curved surface contributes to the majority of aging of the insulation surface, producing over 3000 Joules of thermal energy in 3 minutes of arcing.

C. PREVENTION OF ARC DAMAGE IN SALT-FOG CONDITIONS

This study is supportive of a number of well-established methods for increasing the ability of polymeric insulators to withstand high pollution environments. It is also noted that the development of electrical arcs on service insulators is a complex process involving many factors such as shape, position, electric field distribution, and the natural environment.

It is found that leakage current plays a key role in the growth of dry-band arcs, particularly in salt-fog conditions, as shown in Figures 2 and 4. To reduce leakage current, increasing the 'creepage distance' of insulators is normally considered. This can be achieved by selecting a longer insulator string, larger or more densely arranged sheds [21], and is standard practice as identified in engineering standards such as IEC/TS 60815-3 'Selection and dimensioning of high-voltage insulators intended for use in polluted conditions'. This technique which improves short-term flashover resulting from exceptionally high leakage currents of over 100 mA, will also reduce low currents and hence reduce long-term aging.

Salt fog plays a key role in the formation and growth of dry-band arcs. Arcs in salt-fog conditions tend to have higher accumulated energy radiation when compared with clean fog, as shown in Figure 12 and Figure 14 (d). The increased hydrophobicity of an insulator surface reduces leakage current, which in turn reduces the likelihood of arcing activities on insulators in coastal areas [22]–[24]. Another solution, also associated with preventing flashover events in extreme situations, could be the regular cleaning of insulators in offshore electricity distribution areas, to wash off the salt residues on the insulator surface, preventing the high

conductivity of surfaces when they become wet. High pressure jet washing could be considered when transmission lines are de-energized for maintenance.

It has also been proposed to paint semi-conductive coatings on insulator sheds. When subject to electric fields, semi-conductive materials generate heat, and hence avoid fog deposition on insulation surfaces by Joule heating [25], [26].

VI. CONCLUSIONS

Electrical arc discharges under distribution voltage levels (10kV - 50kV) are of great concern for the reliability and operability of the electricity distribution network. In this paper, the development of low-current dry-band arcs is investigated in both clean-fog and salt-fog conditions, focusing on the potential for long-term damage to polymeric surfaces. Arc features including their formation and stability, arc voltage, current, power, energy and heat dissipation have been studied. The following conclusions are drawn:

1. The time from conditions which allow a first arc to strike, to the situation where the arc is electrically and spatially stable on the insulator surface (time-to-arc-stability) has been identified as a potentially critical parameter in controlling aging of an insulation surface. The time from the initial appearance of an arc to full stability is eight times shorter in a salt fog of 16,000 μS/cm compared to a clean fog of 600 μS/cm, indicating a faster arc development process in salt-fog conditions. This means the very existence of a stable low-current arc is much more likely in polluted conditions.

2. Arcs are more stable in salt-fog conditions rapidly forming one single arc at a fixed location, while arcs in clean fogs tend to diversify into several smaller unstable arcs.

3. Accumulated arc energy in the salt-fog conditions used in these experiments tends to be 150% higher than that in the clean fog under the same source voltage. This is due to the higher arc current present in salt-fog conditions.

4. Using a cylindrical arc model, directional heat dissipation analysis shows that more than 90% of arc energy flows through the curved surface of the cylinder, which has a direct aging contribution to the material surface.

5. Several recommendations are proposed to reduce the likelihood of surface damage in offshore electricity distribution networks likely to experience salt-fog conditions. These are consistent with present design practices to reduce flashover likelihood in polluted conditions.

REFERENCES

[1] D. Zhang, Z. Zhang, X. L. Jiang, Z. Yang, Y. Liu, and M. Bi, "Study on the flashover performance of various types of insulators polluted by nitrates," *IEEE Trans. Dielectr. Electr. Insul.*, vol. 24, no. 1, pp. 167–174, Jan. 2017.

[2] M. Albano, R. T. Waters, P. Charalampidis, H. Griffiths, and A. Haddad, "Infrared analysis of dry-band flashover of silicone rubber insulators," *IEEE Trans. Dielectr. Electr. Insul.*, vol. 23, no. 1, pp. 304–310, Jan. 2016.

[3] N. Dhahbi-Megriche and A. Beroual, "Self-consistent multi-arcs dynamic model for high voltage polluted insulators," *IEEE Trans. Dielectr. Electr. Insul.*, vol. 23, no. 5, pp. 2899–2907, May 2016.

[4] S. M. Rowland, J. Robertson, Y. Xiong, and R. Day, "Electrical and material characterization of field-aged 400 kV silicone rubber composite insulators," *IEEE Trans. Dielectr. Electr. Insul.*, vol. 17, no. 2, pp. 375–383, Apr. 2010.

[5] S. M. Rowland, K. Kopsidas, and X. Zhang, "Aging of polyethylene ADSS sheath by low currents," *IEEE Trans. Power Del.*, vol. 25, no. 2, pp. 947–952, Apr. 2010.

[6] M. Kumosa, L. Kumosa, and D. Armentrout, "Failure analyses of nonceramic insulators. Part I: Brittle fracture characteristics," *IEEE Electr. Insul. Mag.*, vol. 21, no. 3, pp. 14–27, May 2005.

[7] J. S. T. Looms, *Insulators for High Voltages*. London, U.K.: Peregrinus, 1990.

[8] Z. Jia, C. Chen, X. Wang, C. Yang, T. Li, and H. Lu, "Leakage current analysis on RTV coated porcelain insulators during long term fog experiments," *IEEE Trans. Dielectr. Electr. Insul.*, vol. 21, no. 4, pp. 1547–1553, Aug. 2014.

[9] S. H. Kim, E. A. Cherney, and R. Hackam, "Artificial testing and evaluation of RTV coatings in a salt-fog chamber," *IEEE Trans. Electr. Insul.*, vol. 26, no. 4, pp. 797–805, Aug. 1991.

[10] R. S. Gorur, G. G. Karady, A. Jagota, M. Shah, and B. C. Furumasu, "Comparison of RTV silicone rubber coatings under artificial contamination in a fog chamber," *IEEE Trans. Power Del.*, vol. 7, no. 2, pp. 876–882, Feb. 1991.

[11] A. Haddad *et al.*, "A new approach to anti-fog design for polymeric insulators," *IEEE Trans. Dielectr. Electr. Insul.*, vol. 17, no. 2, pp. 343–350, Apr. 2010.

[12] B. Dong, X. Jiang, Z. Zhang, J. Hu, Q. Hu, and L. Shu, "Effect of environment factors on ac flashover performance of 3 units of polluted insulator strings under natural fog condition," *IEEE Trans. Dielectr. Electr. Insul.*, vol. 21, no. 4, pp. 1926–1932, Aug. 2014.

[13] M. Albano, R. T. Waters, P. Charalampidis, H. Griffiths, and A. Haddad, "Infrared analysis of dry-band flashover of silicone rubber insulators," *IEEE Trans. Dielectr. Electr. Insul.*, vol. 23, no. 1, pp. 304–310, Feb. 2016.

[14] I. Ramirez, S. H. Jarayam, and E. A. Cherney, "Performance of silicone rubber nanocomposites in salt-fog, inclined plane, and laser ablation tests," *IEEE Trans. Dielectr. Electr. Insul.*, vol. 17, no. 1, pp. 206–213, Jan. 2010.

[15] A. H. El-hag, S. H. Jayaram, and E. A. Cherney, "Effect of insulator profile on aging performance of silicone rubber insulators in salt-fog," *IEEE Trans. Dielectr. Electr. Insul.*, vol. 14, no. 2, pp. 352–359, Apr. 2007.

[16] S. Kumagai, B. Marungsri, H. Shinokubo, R. Matsuoka, and N. Yoshimura, "Comparison of leakage current and aging of silicone rubbers and porcelain in both field and salt-fog tests," *IEEE Trans. Dielectr. Electr. Insul.*, vol. 13, no. 6, pp. 1286–1302, Jun. 2006.

[17] M. A. Douar, A. Beroual, and X. Souche, "Assessment of the resistance to tracking of polymers in clean and salt fogs due to flashover arcs and partial discharges degrading conditions on one insulator model," *IET Generat., Transmiss. Distrib.*, vol. 10, pp. 986–994, Oct. 2016.

[18] X. Zhang and S. M. Rowland, "The stability and energy of low current surface discharges on wet surfaces," *IEEE Trans. Dielectr. Electr. Insul.*, vol. 19, no. 6, pp. 2055–2062, Jun. 2012.

[19] X. Zhang, S. M. Rowland, and V. Terzija, "Increased energy in stable dry-band arcs due to length compression," *IEEE Trans. Dielectr. Electr. Insul.*, vol. 17, no. 2, pp. 473–480, Apr. 2010.

[20] P. Borkowski and E. Walczuk, "Thermal models of short arc between high current contacts," *Proc. 47th IEEE Holm Conf. Elect. Contacts*, 2001, pp. 259–264.

[21] M. A. Salam *et al.*, "Study of creepage distance of the contaminated insulator in correlation with salt deposit density," in *Proc. Annu. Rep. Conf. Elect. Insul. Dielectr. Phenomena*, 2000, pp. 215–217.

[22] I. Ahmadi-Joneidi, A. Majzoobi, A. A. Shayegani-akmal, H. Mohseni, and J. Jadidian, "Aging evaluation of silicone rubber insulators using leakage current and flashover voltage analysis," *IEEE Trans. Dielectr. Electr. Insul.*, vol. 20, no. 3, pp. 212–220, Mar. 2013.

[23] S. Braini, A. Haddad, and N. Harid, "The performance of nano-coating for high voltage insulators," in *Proc. 46th Int. Univ. Power Eng. Conf. (UPEC)*, 2011, pp. 1–4.

[24] Z. Jia, H. Gao, Z. Guan, L. Wang, and J. Yang, "Study on hydrophobicity transfer of RTV coatings based on a modification of absorption and cohesion theory," *IEEE Trans. Dielectr. Electr. Insul.*, vol. 13, no. 6, pp. 1317–1324, Jun. 2006.

[25] X. Wei, X. Peng, Z. Jia, Z. Sun, and Z. Guan, "Performance of insulators treated with semiconductive silicone rubber coating during fog and polluted conditions," in *Proc. IEEE Int. Power Modulator High Voltage Conf. (IPMHVC)*, Jun. 2012, pp. 439–442.

[26] A. Michalik, S. Tzavalas, B. Singh, and H. D. Le, "Semiconductive polymeric coatings for outdoor polymeric insulation," *IEEE Trans. Dielectr. Electr. Insul.*, vol. 23, no. 3, pp. 1402–1408, Mar. 2016.

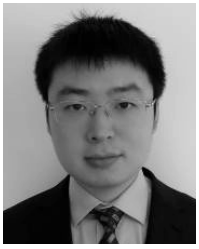

XIN ZHANG (S'08–M'17) was born in Shandong, China. He received the B.Eng. degree in automation from Shandong University, China, in 2007, the M.Sc. and Ph.D. degrees in electrical power engineering from The University of Manchester, U.K., in 2007 and 2010, respectively.

He is a Senior Power System Engineer with the Electricity National Control Centre, National Grid UK. He is currently responsible for generation scheduling and technical analysis of the GB power system, and was involved in the areas of electricity network planning and market operation. He gained valuable industrial experience in the technical and commercial aspects of power transmission and distribution systems. His research interests include intelligent methods in power system planning and operation, smart distribution networks with the integration of renewable and multi-vector energy sources.

Dr. Zhang is a member of the CIGRE SC B5 Protection and Automation working group. He is a Chartered Engineer with the U.K. Engineering Council, a Professional Registration Interviewer and a Professional Registration Advisor to interview and advise Chartered Engineer and Incorporated Engineer applicants for professional registration with U.K.

JIEBEI ZHU (M'13) received the B.S. degree in microelectronics from Nankai University, Tianjin, China, in 2008, and the M.Sc. and Ph.D. degrees in electronic and electrical engineering from the University of Strathclyde, Glasgow, U.K., in 2009 and 2013, respectively.

He joined as a Power System Modeling Engineer with National Grid UK in 2013, and later on involved as a Transmission Network Development Strategy Engineer. He also acted as an Electricity National Control Room Engineer responsible for Scotland transmission real-time security. He is currently with School of Electrical and Information Engineering, Tianjin University, China. His research interests include wind power generation, VSC-HVDC transmission system, ESS, and microgrid dc applications.

SIQI BU (S'11–M'12–SM'17) received the Ph.D. degree from the Electric Power and Energy Research Cluster, The Queen's University of Belfast, Belfast, U.K., in 2012, where he is currently pursuing the Ph.D. degree.

He joined as a Power System Engineer with National Grid UK and then became an experienced U.K. National Transmission System Planner and Operator. He is an Assistant Professor with The Hong Kong Polytechnic University, Hong Kong, and also a Chartered Engineer with U.K. Engineering Council, London, U.K. He has received various prizes due to excellent performances and outstanding contributions in operational and commissioning projects during the employment with National Grid UK and the Outstanding Reviewer Award from the IEEE TRANSACTIONS ON POWER SYSTEMS and the IEEE TRANSACTIONS ON SUSTAINABLE ENERGY. His research interests include power system stability analysis and operation control, including wind power generation, PEV, HVDC, FACTS, ESS, and VSG.

QI LI (AKA STEVEN) was born in Hunan, China, in 1984. He received the B.Eng. degree in electrical and electronics engineering from the University of Birmingham and the Huazhong University of Science and Technology, in 2007, as an Exchange Student, and the M.Sc. degree (Hons.) in electrical power engineering and the Ph.D. degree from The University of Manchester in 2009 and 2013, respectively.

Dr. Li was a Research Associate with the National Grid High Voltage Research Centre, The University of Manchester, U.K., from 2013 to 2016. He then joined as a Power System Engineer in network access planning, network capability electricity at National Grid Plc in 2016. His main research interests include finite-element analysis in high voltage application (electric field calculation for OHL conductors and treeing in underground cables), audible noise evaluation for OHL conductors, corona discharges, and the applications of novel dielectric materials for future power systems.

VLADIMIR J. TERZIJA (M'95–SM'00–F'16) was born in Donji Baraci, Bosnia and Herzegovina. He received the Dipl-Ing., M.Sc., and Ph.D. degrees in electrical engineering from the University of Belgrade, Belgrade, Serbia, in 1988, 1993, and 1997, respectively.

From 1997 to 1999, he was an Assistant Professor with the University of Belgrade, Belgrade, Serbia. From 2000 to 2006, he was a Senior Specialist for switchgear and distribution automation with ABB AG Inc., Ratingen, Germany. Since 2006, he has been with the School of Electrical and Electronic Engineering, The University of Manchester, Manchester, U.K., where he is currently the Engineering and Physical Science Research Council Chair Professor of power system engineering. His current research interests include smart grid application of intelligent methods to power system monitoring, control, and protection, wide-area monitoring, protection, and control; switchgear and fast transient processes, and digital signal processing applications in power systems.

Prof. Terzija is an Editor-in-Chief of the *International Journal of Electrical Power and Energy Systems*, a China One Thousand Talents Plan Scholar, an Alexander von Humboldt Fellow, and a DAAD and Taishan Scholar.

SIMON M. ROWLAND (F'14) was born in London, U.K. He received the B.Sc. degree in physics from The University of East Anglia and the Ph.D. degree from London University, U.K.

He has involved in dielectrics and their applications for many years and has been the Technical Director with multinational companies. He joined The School of Electrical and Electronic Engineering, The University of Manchester, in 2003, where he was an appointed Professor of electrical materials in 2009 and the Head of the school in 2015.

Prof. Rowland was the President of the IEEE Dielectric and Electrical Insulation Society in 2011 and 2012.